Geodinamica Acta 21/4 (2008) 187-202

Geodinamica Acta

Late Quaternary episodic displacement on a sackung scarp in the central Spanish Pyrenees. Secondary paleoseismic evidence?

Francisco Gutiérrez[1*], María Ortuño[2], Pedro Lucha[1], Jesús Guerrero[1], Enrique Acosta[1], Paola Coratza[3], Daniela Piacentini[3], Mauro Soldati[3]

[1] *Edificio Geológicas, Universidad de Zaragoza, C/ Pedro Cerbuna 12, 50009 Zaragoza, Spain*

[2] *Departamento de Geodinámica y Geofísica, Universitat de Barcelona, Spain*

[3] *Dipartimento di Scienze della Terra, Università di Modena e Reggio Emilia, Italy*

Received: 29/03/2008, accepted: 24/09/2008

Abstract

A sackung scarp has been investigated by trenching in the central Spanish Pyrenees. This feature is located 18 km to the SW of the North Maladeta Fault, which is the most probable source of the M_w 5.3 Vielha earthquake of 1923. Three displacement events have been inferred for the trenched sackung based on colluvial wedge stratigraphy and fault truncation. The increasing amount of deformation in each successive faulting event may be related to the progressive weakening of the slope through time. A minimum vertical slip rate of 0.19 mm/yr has been calculated for the sackung scarp. Several arguments suggest that the episodic displacement of the analysed sackung is controlled by strong seismic shaking: (a) Spatial association of the sackung features with the North Maladeta Fault; (b) Episodic displacement with a millennial recurrence (5.6 kyr) consistent with the expectable earthquake recurrence interval for a low slip rate fault, like the neighbouring North Maladeta Fault. Demonstrating in future investigations that the sackung features in the area constitute archives of large paleoearthquakes would be of great interest for seismic hazard assessments. They might help to improve the catalogue of paleoearthquakes and might provide information on earthquake recurrence intervals and the age of the most recent event (MRE).

Keywords: sackung, antislope scarp, trenching, paleoearthquakes, Spanish Pyrenees

1. Introduction

Gravitational spreading in rock slopes may be accommodated through the development of failure planes dipping into the slopes with extensional dip-slip displacement. These brittle structures, generally parallel to the ridge crests and contour lines, produce uphill-facing scarps (also called antislope scarps, counter scarps and antithetic scarps) and linear depressions lying at their foot. The scarps in the ridge tops may create double or twin ridges and ridge top depressions. These linear geomorphic features are collectively designated by numerous authors as sackung [1, 2, 3, 4]. Other landforms commonly found in association with sackung include: (a) A bulge at the toe of the slope. The oversteepened lower portion of the slope is frequently affected by landslides (e.g. [5, 6, 7]), (b) Downhill-facing scarps including large concave scarps that resemble the head scar of a landslide [8, 2, 7, 9, 4], (c) Extensional fissures [10, 11, 12, 13], (d) Saddles and notches in secondary ridges [2], and (e) Small sinkholes [14, 10, 2].

* Corresponding author.
E-mail address: : fgutier@unizar.es
Tel.: 34 976 761090 - *fax:* 34 976 761088

doi:10.3166/ga.21.187-202

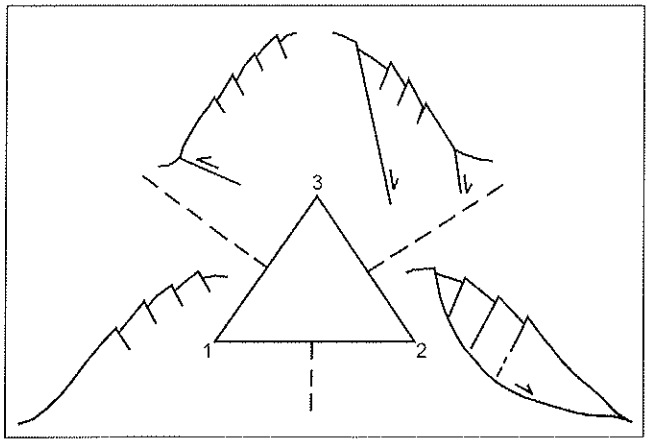

Fig. 1: Ternary diagram illustrating three end-members of slopes with sackung features: **(1)** Sackung failure planes that grade downwards into a continuous deformation. **(2)** Antithetic sackung failures connected to the sliding surface of a deep-seated landslide. These two extremes may represent a temporal gradation. **(3)** Sackung failures that correspond to secondary ruptures associated to active faults.

The uphill-facing scarps are typically tens or hundred meters long and a few meters high [15], and generally display height/length ratios significantly higher than tectonic fault scarps [3]. The troughs accompanying the antislope scarps may host closed depressions with ponds which constitute areas of deposition. Several studies illustrate that information on the chronology and kinematics of sackung structures can be inferred studying the stratigraphy, structure and geochronology of the sediments filling these sediment traps (e.g. [2, 9]).

Three main mechanisms involving gravitational deformation in the slopes have been proposed to explain the development of uphill-facing scarps [4]: (a) Differential downslope bending of rocks affected by steeply dipping discontinuity planes [16]. (b) Flexural slip toppling of rock slabs defined by joints steeply dipping into the slopes [14, 10]. (c) Normal dip-slip displacement on failure planes dipping into the slopes. Sliding on these structures produces the lateral spreading of the ridge flanks and subsidence in the ridge crests (e.g. [1, 17]). This mechanism, acting alone or in combination with toppling, is probably the one that provides the most satisfactory explanation for the majority of the sackung features documented in the literature.

Some authors consider that the sackung failure planes are accommodated downwards by continuous creep deformation [5]. Others propose that they merge with deep-seated and well-defined sliding surfaces, forming part of a "normal" landslide [18, 7, 19, 20]. Some researchers infer their connection and genetic relation with active tectonic faults (e.g. [21, 22, 23, 24, 25]). Probably, a complete spectrum may exist between these three end-members [9, 4, 26], which could be represented in the apexes of a triangle (Fig. 1).

Three main displacement regimes may be conceived for the sackung failure planes; continuous slow creep, rapid episodic displacement, and gradual creep movement punctuated by discrete events of displacement. Information on the short- and long-term kinematics of particular sackung features has been obtained by means of high resolution geodetic measurements and studying the sediments filling the sackung troughs by trenching. In Bald Eagle Mountain (Rocky Mountains of Colorado) and in Mosaic Ridge (southern Coast Mountains, British Columbia), overall maximum rates of horizontal displacement of approximately 4 and 40 mm/year, have been measured, respectively [27, 28, 10]. Geodetic studies carried out by Bovis and Evans [29] yield vertical slip rates of up to 10 mm/year in particular antislope scarps in the British Columbia. Continuous displacement on sackung failure planes may be recorded by progressive synsedimentary deformation (cumulative wedge-outs) in the sackung trough sediments [2, 30]. Conversely, colluvial wedges, angular unconformities and different generations of fissure fills constitute stratigraphic evidence of instantaneous displacement events [31, 32, 3, 12, 13, 9, 19, 4]. An additional interest of sackung features is that they have been identified in slopes that have failed catastrophically producing rock avalanches ([33] and references therein).

Sackung features have been described in a wide variety of geologic environments, including volcanoes [6, 34] and mountain ranges bounding graben depressions in Valles Marineris in Mars [35]. However, these manifestations of lateral spreading are particularly frequent in glaciated and seismically active mountain ranges [6]. Regarding the dynamics of the sackung scarps, most of the authors claim for three main sources of stresses: (a) Unloading related to glacier retreat in valleys with oversteepened slopes (e.g. [7] and in plateaus [36]). (b) Tensional stresses induced by gravity in steep-sided ridges [37, 38]. (c) Strong seismic shaking (e.g. [18, 11, 39, 9, 40, 4, 41]), which may be enhanced by topographic amplification [42].

The idea of the causal and chronological relationship between sackung features and earthquakes is gaining advocates with the increasing number of accounts that document the generation and reactivation of sackung scarps during large historic earthquakes. Ridge top sackung scarps in Stillwater Range, central Nevada, experienced displacement during the 1915 Pleasant Valley earthquake (M_s 7.6) and the 1954 Dixie Valley-Fairview Peak earthquakes (M_s 6.8 and 7.2), and as many as six displacement events have been inferred by trenching across one of the scarps [43, 44]. McCalpin and Hart [9] present a partial compilation of nine localities in California where the occurrence of sackung features associated with 5 historic earthquakes with magnitudes ranging from M 5.9 to M 8, has been reported (San Francisco 1906, San Fernando 1971, North Palm Springs 1986, Loma Prieta 1989, and Northridge 1994). In some sackung features, recurrent displacement accompanied two of those seismic events. Trenching across sackung scarps and depressions reactivated during the M_w 7.1 Loma Prieta earthquake of 1989, revealed evidence of prehistoric displacements similar in style and magnitude to that caused by that seismic event [45, 46]. Some other historic earthquakes that have induced the formation or reactivation of sackung scarps include: (a) The Alaska earthquakes of 1899, 1958 (M 7.9) and 1964 (M_w 9.2) ([47];

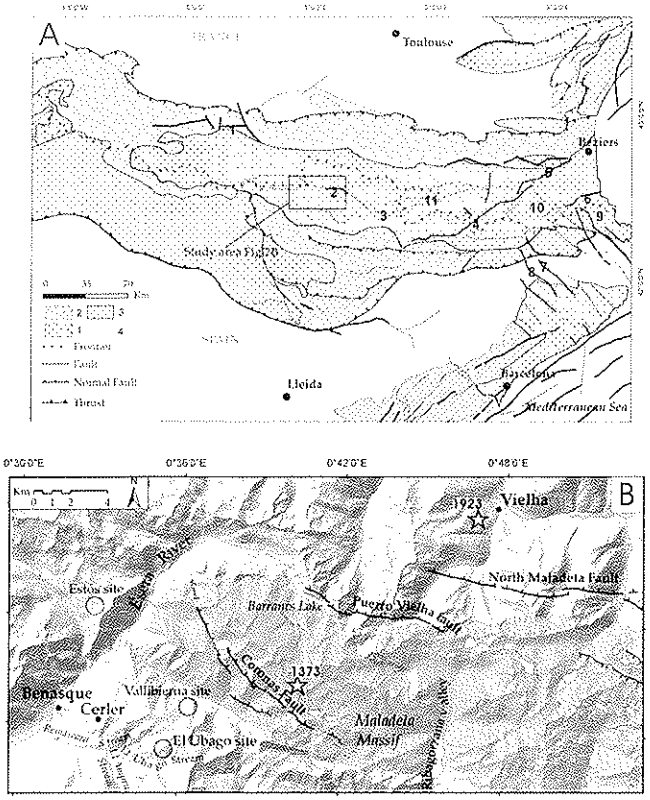

Fig. 2: A. Geological and tectonic sketch of the Pyrenees. Geological units: a. Paleozoic basement, b. Mesozoic cover, c. Synorogenic Tertiary cover, d. Neogene and Quaternary cover. Faults and tectonic basins: 1. Lourdes, 2. North Maladeta, 3. Tirvia, 4. Cerdanya-Conflent, 5. Tet, 6. Tech, 7. Empordà, 8. Amer, 9. Alberes, 10. Canigou, 11. Urgellet-Escaldes. B. Digital elevation model of the area indicated in A showing the location of the El Ubago, Vallibierna and Estós sites and the main physiographic and structural features mentioned in the text. The non-shaded area with a light grey tone corresponds to the Maladeta granodioritic batholith. The Vielha (1929) earthquake and the Ribagorza (1373) earthquake have been marked with star symbols.

[48]; [49]); (b) The M 7.9 Denali Fault earthquake of 2002 [50]; (c) The earthquake that struck Central Italy in 1703 [51]; (d) The 1980 Irpina (Italy, M 6.9) and El Asnam (Algeria, M_s 7.2) earthquakes [52]; (e) The M_w 5.7-6 Umbria-Marche (Apenines) seismic sequence of 1997 [53]; (f) Possibly, the Chile earthquake of 1835 [54].

Demonstrating in a particular area that the kinematics of sackung features is controlled by earthquake shaking events would require: (a) identifying evidence of episodic displacement in the sackung features; (b) obtaining tight absolute dates for those displacement events; (c) establishing the contemporaneity of the displacement events between different sackung features, and especially with independently-dated earthquakes [9]. Testing this hypothesis could be of great interest for seismic hazard assessments, since investigation of sackung features might allow improving the paleoseismic catalogues and providing estimates of earthquake recurrence intervals. Such a record of secondary paleoseismic evidence would be of special utility in areas where seismogenic faults are buried, blind or have poor geomorphic expression. McCalpin and Hart [9] identified stratigraphic evidence of 2-4 prehistoric displacement events in 3 trenches dug across ridge top sackung depressions close to the San Andreas and San Gabriel Faults in California. However, the age brackets for these events where too old, or not tight enough to make a satisfactory correlation with any particular paleoearthquake. The time brackets for the sackung faulting events overlapped several prehistoric earthquakes or were older than the available paleoearthquake chronologies derived from trench studies.

In a previous work, Gutiérrez-Santolalla *et al.* [4] analysed sackung features in the neighbouring Estós and Vallibierna glacial valleys, in the Spanish Pyrenees. Trenching across a sackung trough in each of these valleys and radiocarbon dating of sediments provided the following findings: (a) The formation of the sackung troughs and scarps, at ca. 5.9 and 7.6-7.8 ka in Vallibierna and Estós sites, respectively, occurred more than 5 kyr after the deglaciation of the valleys (16-13 ka); (b) Upward fault truncation by undeformed deposits in the trough fill of Vallibierna site provides evidence of a faulting event occurred between 5.6-2.7 ka suggesting that the kinematics of this sackung has been governed by an episodic displacement regime. Based on these data, the authors hypothesized that although debutressing of the valley walls by deglaciation predisposed the slopes to sackung formation, the creation and development of these features was controlled by strong seismic shaking.

In this work we analyse the sackung features developed in the El Ubago glacial valley and present the results of a trench dug across an uphill-facing scarp and trough. The trench was placed at a distance of 2.2 km from the Vallibierna trench site, on the opposite flank of the same ridge (Fig. 2). One of the main reasons for selecting the El Ubago valley, situated very close to the previously studied sackung features, was to obtain additional data on sackung development in the area which could be compared with the results presented in the previous study. The new information could help to reinforce or challenge our previous interpretations. The aim of the work is to (a) characterise the geomorphology of the sackung features in the El Ubago valley, (b) infer the kinematic history of the trenched sackung constraining the timing of its initiation and subsequent displacement, and (c) compare these results with the poorly constrained available glacial chronologies and with those obtained from the Vallibierna and Estós sites.

2. Geological setting, neotectonics and seismic activity

The Pyrenees, with a dominant WNW-ESE structural and topographic grain, is an Alpine orogen resulting from the collision of the Iberian and European plates from Upper Cretaceous to Miocene times. The study area is located in the so-called Axial Zone of the Pyrenees, which constitutes the topographic core of the mountain range [55]. This geological unit, interpreted as the crestal area of an antiformal structure generated by the stacking of south-verging Alpine thrusts [55],

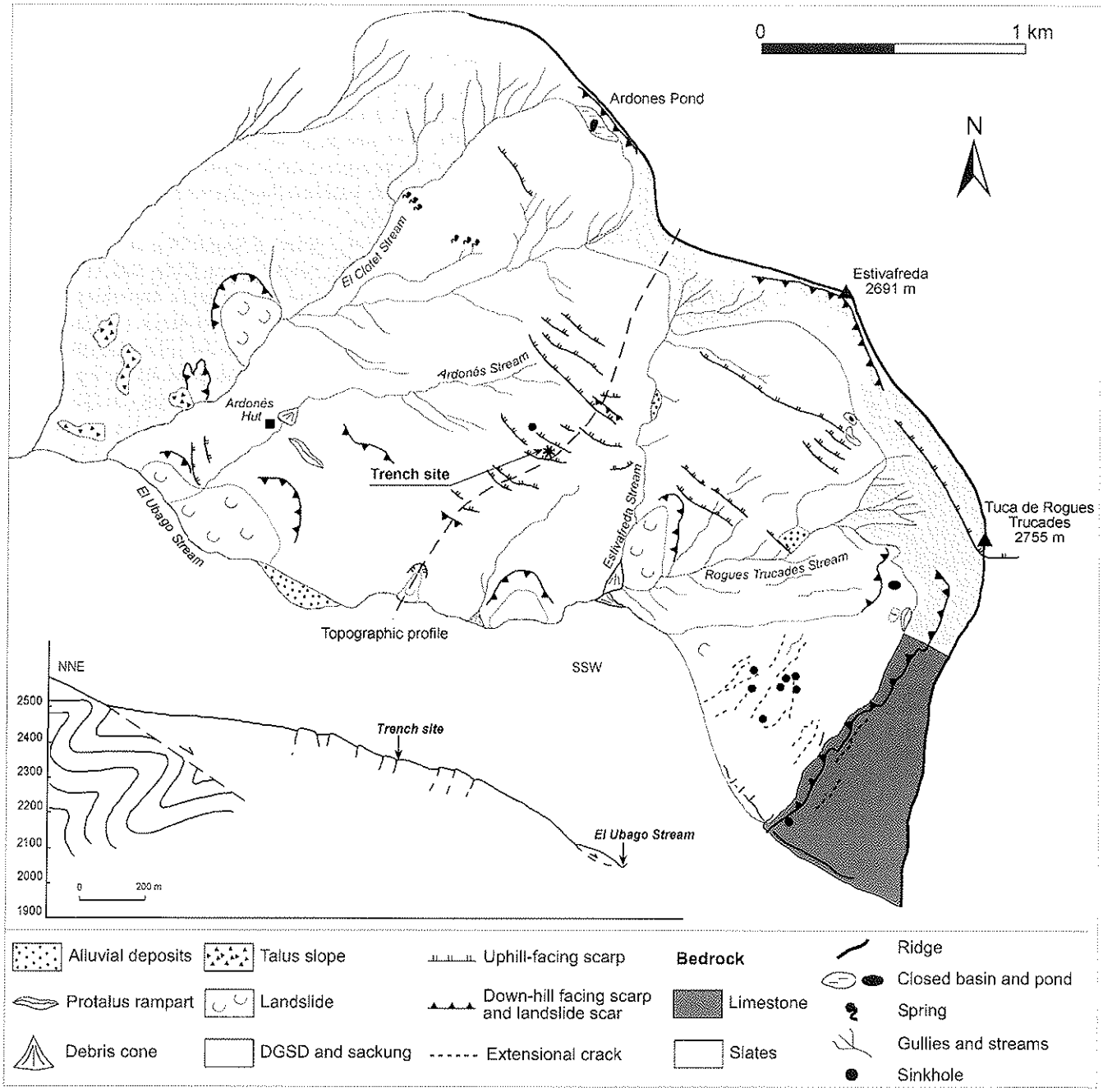

Fig. 3: Geomorphological sketch of the northern slopes of the El Ubago glacial valley showing the location of the trench and the trace of the topographic profile of the inset figure.

constitutes a major basement outcrop consisting of strongly deformed Paleozoic sedimentary and metasedimentary rocks (affected by the Variscan and Alpine orogenies) and late Variscan granodioritic plutons [56, 57, 58].

The Pyrenees cannot be considered as an active plate margin since the present-day rate of convergence obtained by means of GPS measurements does not exceed 0.5 mm/yr [59]. However, the Pyrenean range is one of the most seismically active areas in Western Europe [60] and has been the scenario of destructive earthquakes in the past [61, 62, 63], some of them of M_w >6.

The post-orogenic tectonic evolution of the Pyrenees has not yet been well deciphered. High-precision levelling [64] and GPS data analyses [59, 65] are being performed but do not provide reliable enough records about relative movements across the chain. The available information on the neotectonic regime of the Pyrenees come from 1) evidence of late Miocene to Quaternary active tectonics and 2) data derived from borehole breakouts and focal mechanism solutions. These latter data have been recently analysed by Sitch *et al.* [65] and De Vicente *et al.* [66], showing that the Pyrenean range is dominated by extension, except in the easternmost part, in which they infer a strike-slip regime.

The neotectonic activity observed in the Eastern and Western parts of the range shows a variety of faulting regimes. In the Western sector, the Lourdes Fault is the structure with a major concentration of minor and moderate seismic events. Thrust faulting and normal faulting associated to flexural slip along this E-W oriented and S-dipping fault [67] and right lateral strike-slip faulting [63] have both been proposed to explain the deformation. In the surroundings of this system, some other evidences of recent tectonic activity have been found [68, 69]. At the Eastern sector, the stratigraphic and geomorphic evidence of neotectonic activity is more abundant, indicating and E-W extension followed by N-S compression. This evolution led to the formation of neotectonic basins controlled by faults with geomorphic expression such as the Empordà, Tech, Amer (also known as Brugent), the Urgellet-Escaldes and Tet-Cerdanya-Conflent fault systems [e.g. 70, 71, 72, 73].

Despite the reported evidences of neotectonic activity along faults with geomorphological expression, there is a noticeable lack of paleoseismic data.To our knowledge, the only data on paleoearthquakes obtained by trenching across a fault in the Pyrenees are those published by Alasset and Meghraoui [67] at the Lourdes Fault. Information on secondary paleoseismic evidence is also scarce. Rodríguez-Pascua [74] has documented three Late Quaternary stratigraphic levels with paleoseismites in the Tirvia glacio-lacustrine basin, about 60 km E of the study area.

In the central Spanish Pyrenees, the E-W trending North Maladeta Fault, located about 18 km to the NE of the study area, has been identified as the most probable source of the M_w 5.3 Vielha earthquake of 1923, and as a possible source for the Ribagorza earthquake of 1373 [75, 76], with an estimated magnitude of M_w 6.2 [77, 62]. However, no evidence of recent surface rupture has been found associated to this structure, whose geomorphic expression can be traced for at least 17.5 km (Fig. 2). Its activity as a normal fault has been recorded since the Late Miocene, with a maximum vertical slip rate of 0.06-0.08 mm/yr [76]. Based on the mappable length of the fault trace (17.5 km) and applying the empirical relationships of Wells and Coopersmith [78], a potential magnitude of M_w 6.5±0.3 has been estimated by Ortuño *et al.* [76] for the maximum earthquakes that could generate this fault.

In the Maladeta granodioritic massif, 4 km to the NE of the studied sackung features, several antislope scarps 3-6 km long [79] and the 300 m long scarp of the Puerto de Vielha Fault [8] have been attributed to recent reactivations of pre-existing faults, most likely secondary structures. One of these morpho-structures, the Coronas Fault, is located 6 km to the north of the sackung feature analysed in this work (Fig. 2). Regretfully, intense glacial erosion makes difficult the preservation of geomorphic and stratigraphic evidence of surface ruptures, and thus, establishing the timing of the faulting events. In a core from Barrancs Lake, located about 10 km NE of the El Ubago site (Fig. 2), Cruz *et al.* [80] identified two lake lowstands dated at 1540±30 and 2300±40 ^{14}C yr BP. These authors propose that these lowstands, recorded by peat units that interrupt sharply a continuous sedimentation of rythmites and turbidites, represent the sudden desiccation of the lake due to drainage through fractures opened during earthquakes.

The analysed sackung features are located in the northern slopes of the El Ubago glacial valley (Fig. 2). The bedrock, primarily composed of tightly folded Silurian and Lower Devonian black slates with limestone intercalations, constitutes the core of a NW-SE-trending and S-verging anticlinorium. The bedding has a general dip into the slope and strikes roughly parallel to the ridge crest (Fig. 3). Southeast of the Roques Truncades Stream, the slates are overlain by more competent Lower Devonian limestones (Dalle Limestone) affected by folds and thrusts (Fig. 3). This limestone unit reaches a cumulative thickness of ca. 300 m in the El Ubago valley [81].

3. Glacial evolution and geomorphology

The El Ubago glacial valley is located in the Remáscaro drainage basin, excavated on the eastern margin of the main Ésera glacial valley (Fig. 2). This basin, hanged about 300 m above the Ésera valley due to glacial overdeepening, comprises two main subbasins drained by the El Ubago and El Ampriu streams. Both streams join close to Cerler village forming the trunk Remáscaro stream. The evolution of this basin during the last glacial phase has been reconstructed by Bordonau [82] based on geomorphic and stratigraphic evidence, although there is no geochronological data available from the area. According to this author, during the "premaximum phase", before the ice reached its maximum extent (pleniglacial), the Ésera glacial valley dammed the drainage of the Remáscaro watershed, forming a glaciolacustrine basin next to the left lateral moraine of the Ésera glacier and downstream of the El Ubago and El Ampriu local glaciers. In the subsequent "maximum phase", the El Ubago and El Ampriu glaciers joined with the main Ésera glacier overriding and deforming the sediments deposited in the previously existing juxtaglacial-proglacial lake. This phase is recorded by glacial till deposited over strongly deformed glaciolacustrine and glaciofluvial deposits [82]. During the "deglaciation phases", the El Ubago and El Ampriu glaciers disconnected from the Ésera glacier and a new glaciolacustrine basin formed next to the Ésera glacier lateral moraine [82]. Moraine ridges mapped around the junction of the Remáscaro, El Ubago and El Ampriu streams indicate an initial phase in which the El Ubago and the El Ampriu glaciers merged sharing the same terminal moraine, and a later one in which they were separated. In the headwaters of the basin (Ballberdera, Basibé, Gallinero) we have identified recessional moraines which correspond to younger deglaciation phases of unknown age.

An aspect of special interest for our study is to determine the approximate time at which the El Ubago glacier underwent a retreat large enough to leave the studied slopes free of any significant glacial loading. The traditional Late Pleistocene-

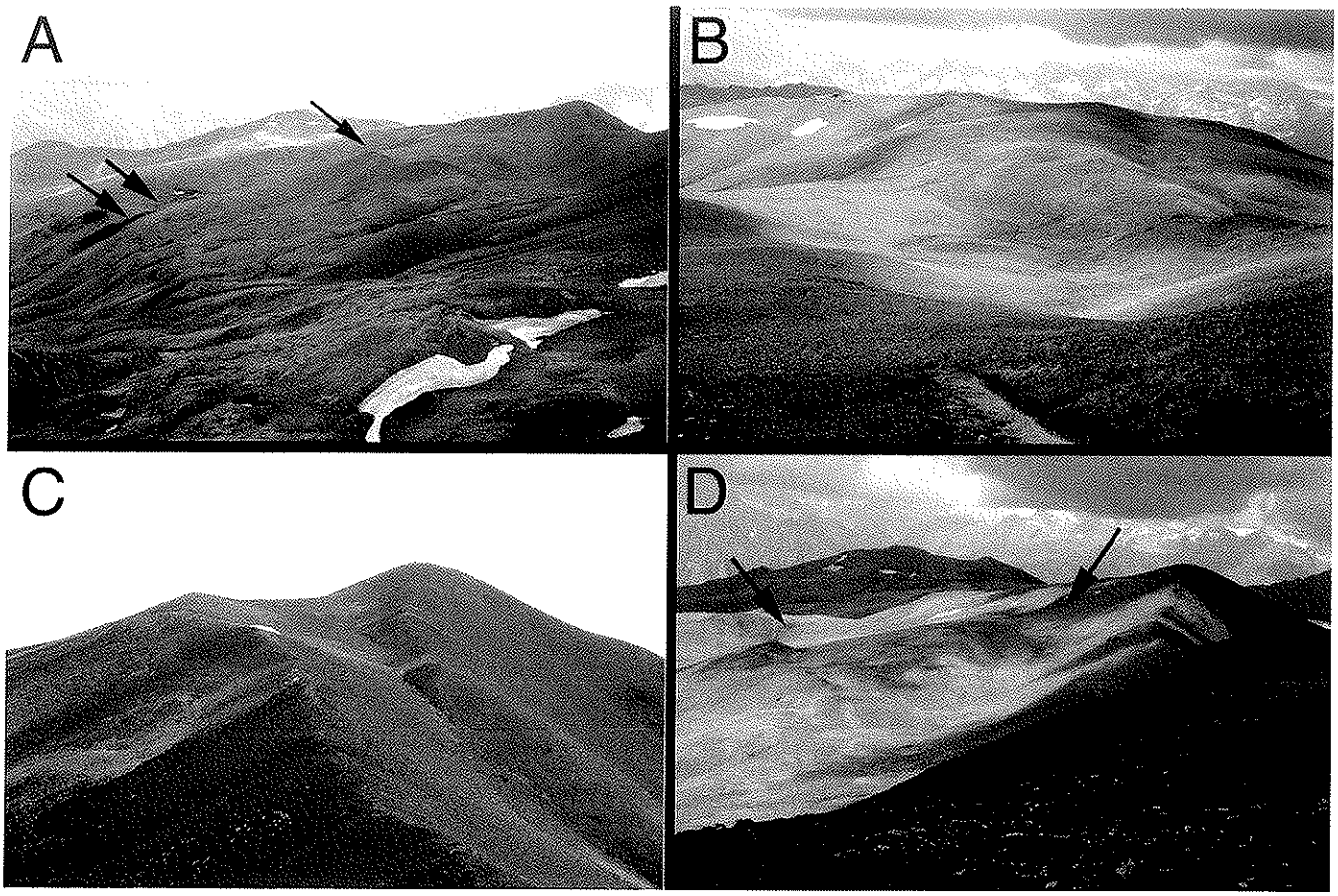

Fig. 4: **(A)** General view of the slopes between the Estivafreda and the Roques Truncades streams. Note the overall convex profile interrupted by a large keystone graben in the upper part. Arrows point to uphill-facing scarps. **(B)** Closed depression and pond (Ardonés Pond) in a ridge top depression NW of Estivafreda Peak. **(C)** Roques Truncades Peak split by a sackung scarp. **(D)** Graben structure flanked by uphill- and downhill-facing scarps in the upper part of the slope located SW of Estivafreda Peak.

Holocene glacial chronology of the Spanish Pyrenees, largely based on radiocarbon datings and morpho-topographic correlations [83], maintain that the Pyrenean glaciers reached the maximum extent (pleniglacial) at around 50-45 ka, long before the global LGM, and that the episodes of "high altitude glaciers" and "cirque glaciers" occurred at 16-15 and 14-13 ka, respectively. According to this chronological scheme, the main retreat of the El Ubago glacier might have occurred between 16 and 13 ka.

Recently, Pallàs *et al.* [84] have proposed a new glacial chronology for the Pyrenees based on some previously reported radiocarbon ages and new ^{10}Be datings from the Noguera Ribagorzana valley, adjacent to the east of the Ésera valley. These authors argue that the traditional chronology is largely based on unreliable radiocarbon dates and that the beginning of the last deglaciation probably occurred after 25 ka. Surface exposure ^{10}Be dating of glacial landforms indicates that the main glacier disappeared before 11.7 ± 1.5 ^{10}Be ka in the Bessiberri glacial trough, a tributary valley of the Noguera Ribagorzana valley. Since the Bessiberi valley has the same orientation as the El Ubago valley but with the headwaters at a higher altitude, according to this chronology, deglaciation in the El Ubago valley should have occurred before 12 ka.

The northern slopes of the El Ubago glacial valley, with a maximum local relief of 700 m, show a conspicuous convex longitudinal profile indicative of post-glacial gravitational deformation (Figs. 3 and 4A). The area affected by landslides and deep-seated gravitational slope deformation [85] covers approximately 4.4 km^2. We estimate a probable volume of about 600 hm^3 for the mass affected by gravitational instability, being one of the largest mass movements documented in the Pyrenees. Based on the geomorphic configuration of the slopes in the El Ubago glacial valley, we estimate that the ice reached a maximum thickness of around 150 m in the stretch in which the studied sackung is located. Considering that the density of the glacial ice is around 0.9 g/cm^3, a stress release of about 13.5 kg/cm^2 (1.3 MPa) can be estimated for the rocks located on the valley bottom.

Southeast of the Roques Truncades stream, where the slates are overlain by a thick limestone unit, the slope shows a complex landslide with clearly identifiable limits (Fig. 3). In the southern sector of the slope, plastic deformation and possibly sliding of the slates have caused the gravitational spreading of the overlying limestone controlled by NE-SW trending joints. The progressive lateral and vertical displacement of the limestone blocks has generated a stepped topography with

NE-SW trending trenches, fissures and sinkhole alignments. In the northern sector of the slope, the slates, devoid of any limestone caprock, show a tongue-shaped landslide at the foot of an arcuate head scarp. It seems that both sliding along well-defined failure planes and flowage are involved in the displacement of this landslide with fresh appearance.

The slopes between the El Clotet and the Roques Truncades streams show obvious geomorphic evidence of gravitational deformation (Fig. 3). To the NW of Estivafreda Peak, the undulating ridge top has a 225 m long depression with a permanent pond (Ardonés Pond) bounded by NW-SE trending downhill- and uphill-facing sackung scarps (Fig. 4B). The Tuca de Roques Truncades Peak is split by a 720 m long upslope-facing scarp ("Roques Truncades" means cut rocks; Fig. 4C). In this sector of the valley the slopes show an anomalous profile. The upper part of the slopes shows a steep downhill-facing scarp up to 90 m high above a relatively flat zone which resemble the head scarp of a landslide (Fig. 4A). In the SW flank of Estivafreda Peak there is a 300 m wide depression with convex topography bounded by an arcuate downhill-facing scarp and an antislope scarp 650 m long (Figs. 3 and 4D). This morphostructure corresponds to a large keystone graben controlled by a deep-seated sliding surface and a NE-dipping antithetic normal fault. Probably, the SW dipping sliding surface does not reach the base of the slope and gives way to a continuous ductile deformation, as suggests the lack of a clear landslide toe at the base of the slope. The intermediate and lower portions of the slopes have a convex profile with a progressive downhill increase in the gradient, which may be related to glacial erosion and post-glacial outward bulging (Figs 3 and 4A). The lower sector of the slopes is affected by some landslides, most likely favoured by the oversteepening induced by gravitational deformation and stream undercutting (Fig. 3).

The uphill-facing scarps have been mapped by means of aerial photograph interpretation and field surveys using 1:18,000 and 1:5,000 scale images. Although they occur along the whole profile of the slopes, they are more frequent in the intermediate sectors (Fig. 3). We have identified 28 uphill-facing scarps ranging from 60 to 720 m in length and with an average length of around 200 m. The great majority of the scarps have a NW-SE trend parallel to the structural and topographic grain, and some show a slight valleyward convexity. Although the maximum height of the scarps is highly variable, reaching more than 5 m, none of them show a fresh appearance. This indicates that they have not experienced noticeable reactivations in recent times. Some sackung scarps control or block the drainage and the associated linear depressions may host small ephemeral ponds (Fig. 3). Locally, some sackung features have been transformed into benches due to degradation of the scarps and aggradation in the troughs, including the accumulation of solifluction lobes (Fig. 5A). The highest concentration of sackung scarps is located between the El Clotet and the Estivafreda streams, where the trench site is located. Here, the slope has a local relief of 500 m and an average gradient of 17° (Fig. 3). In this sector, a fresh collapse sinkhole 1.2 m across and 1 m deep has been mapped on the prolongation of a sackung scarp (Fig. 5B). This subsidence feature may be related to downward migration (suffusion, ravelling) of colluvial deposits through extensional fissures in the bedrock.

Fig. 5: **(A)** Sackung scarp and trough transformed into a bench overridden by active solifluction lobes. **(B)** Fresh cover collapse sinkhole probably related to downward migration of the colluvial deposit through open fractures in the bedrock.

4. The studied sackung scarp and trough

4.1. Geomorphology

The sackung scarp and trough in which we dug the trench is located at 2,380 m in elevation and has a general N105E strike. This sackung feature is associated to another uphill-facing scarp to the NW with a N140E orientation (Figs. 3 and 6). Both features, with an elevation difference of about 10 m, show a left stepping en echelon arrangement with a closed depression in the transfer zone (Fig. 6). The ridge of the trenched sackung has a mostly subdued rounded geometry reaching a maximum height of 1.3 m above the trough. The excavation of the trench revealed that the main failure plane is located approximately beneath the ridge crest, coinciding with a linear change from bare to turf-covered ground (Fig. 7A).

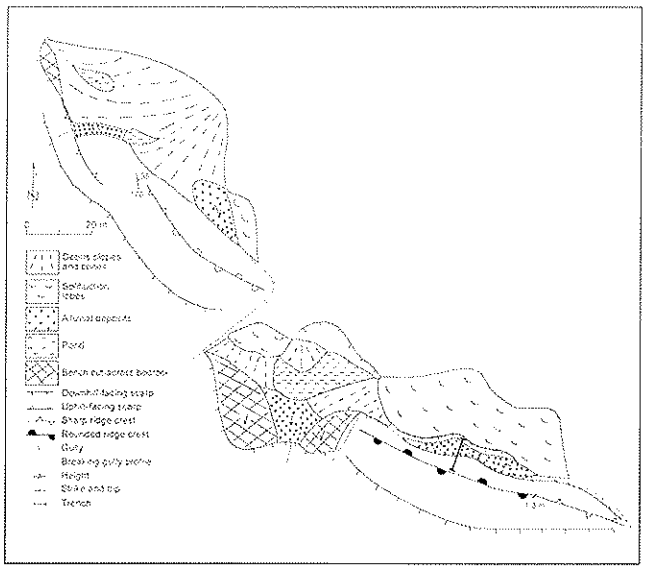

Fig. 6: Detailed geomorphological map of the trenched sackung features. This sketch was produced by direct mapping on graph paper in the field using a laser distanciometer and compass.

The sackung trough is drained by two scarcely incised longitudinal drainages that show a sharp bend in the scarp tips. The bottom of the trough, with a slight ENE inclination, is flanked by scarps a few decimetres high at both sides. The southern scarp seems to be related to fluvial incision and the northern one corresponds to the front of solifluction lobes that have overridden part of the depression (Fig. 6 and 7B).

In the step-over zone, the sackung ridge dies out and is replaced by two nearly flat surfaces cut across bedrock. These benches are interrupted by a very shallow alluvium-covered incision that acts as the spill way of the adjacent pond. The pond is bounded on its northern margin by a prominent downhill-facing scarp (Fig. 6). This could be the surface expression of a synthetic failure plane that accommodates the deformation in the transfer zone. The adjacent sackung shows two ridges with a right stepping arrangement and the trough seems to have been largely covered by colluvium.

4.2. Trenching strategy and methodology

The selection of the trench site (42° 35' 21.91"N; 0° 35' 22.4"E) was based on several reasons, taking into account that the excavation had to be performed by hand: (1) We expected to find failure planes near the surface, since the sackung scarp, with a limited height (1.3 m), did not seem to have a thick colluvial cover; (2) The sackung ridge and trough were relatively narrow; (3) Although there were narrow sackung troughs at a higher elevation with clear evidence of ponding, we thought that it would be more probable to find charcoal at a lower elevation.

The trench, about 10 m long, 3.2 m deep and 0.9 m wide, was oriented perpendicular to the sackung with its southern end coinciding approximately with the sackung ridge. It was excavated using picks, hoes, shovels and buckets. A reference grid with horizontal and vertical strings spaced 0.5 m apart was placed on the SE wall of the trench, which was logged on graph paper. We only found charcoal for AMS radiocarbon dating in three stratigraphic levels (Fig. 8).

4.3. Trench stratigraphy, structure and geochronology

The trench dug across the uphill-facing scarp and the adjacent trough reveals that these landforms have been created by normal dip-slip displacement on at least two major N-dipping faults (F1 and F2) and tilting of the drownthrown blocks (Fig. 8). Fault F1 lies beneath the crest of the rounded sackung ridge and is manifested at the surface by a sharp rectilinear limit in the turf vegetation that covers the unconsolidated sediments of the trough fill and not the footwall bedrock (Fig. 7A). Fault F2, with an attitude of N138E57NE measured in the NW wall of the trench, is located beneath the medial sector of the subdued sackung scarp. This fault plane is coated by a thin film of clay showing striations indicative of pure dip slip displacement (Fig. 9). Three minor N-dipping failures have been also mapped between faults F1 and F2. The top of the bedrock shows a vertical separation of 3.2 m in the trench.

The trough fill reaches 3.0 m in thickness at stations 5.5-6 of the log horizontal scale. A slightly larger thickness may be expected at station 5 where the structural and depositional axis of the trough seems to be located (Fig. 8). Three main sedimentological facies have been identified in the unconsolidated deposits of the sackung trough: (a) Very massive and homogeneous argillaceous pond deposits with granules in which it has been very difficult to differentiate stratigraphic units and breaks due to the scarcity of textural and colour changes. (b) Subangular and poorly sorted pebble and granule gravels shed from the sackung scarp and interpreted as colluvial wedges that record free face formation by rapid displacement events. (c) Roughly stratified and moderately sorted sandy granule and pebble gravels derived from the uphill slope of the sackung trough. This deposit is ascribed to sheetwash and slopewash processes related to severe rainfall events. In the sector of the trench associated to the sackung scarp these facies are arranged in three cyclic depositional sequences consisting of a lower colluvial gravel unit and an upper lacustrine argillaceous unit. These sequences record scarp creation or rejuvenation events with free face formation and colluvial wedge deposition, followed by long quiescence periods of scarp degradation and expansion of lacustrine deposition.

The bedrock exposed in the trench (unit B) is made up of densely jointed and highly fissile ampelitic slates of Silurian age [81]. Bedding shows an apparent dip of about 10-15° towards the trough. About 25 m to the SE of the trench site, stratification in the slates exposed at the sackung ridge is roughly parallel to the orientation of the scarp and dips gently into the slope (N130E10NE). Between the two major faults, we have recognized a 10 cm thick brownish black unit of weathered bedrock (regolith) composed of slate fragments with interstitial clay with no detrital components (unit R).

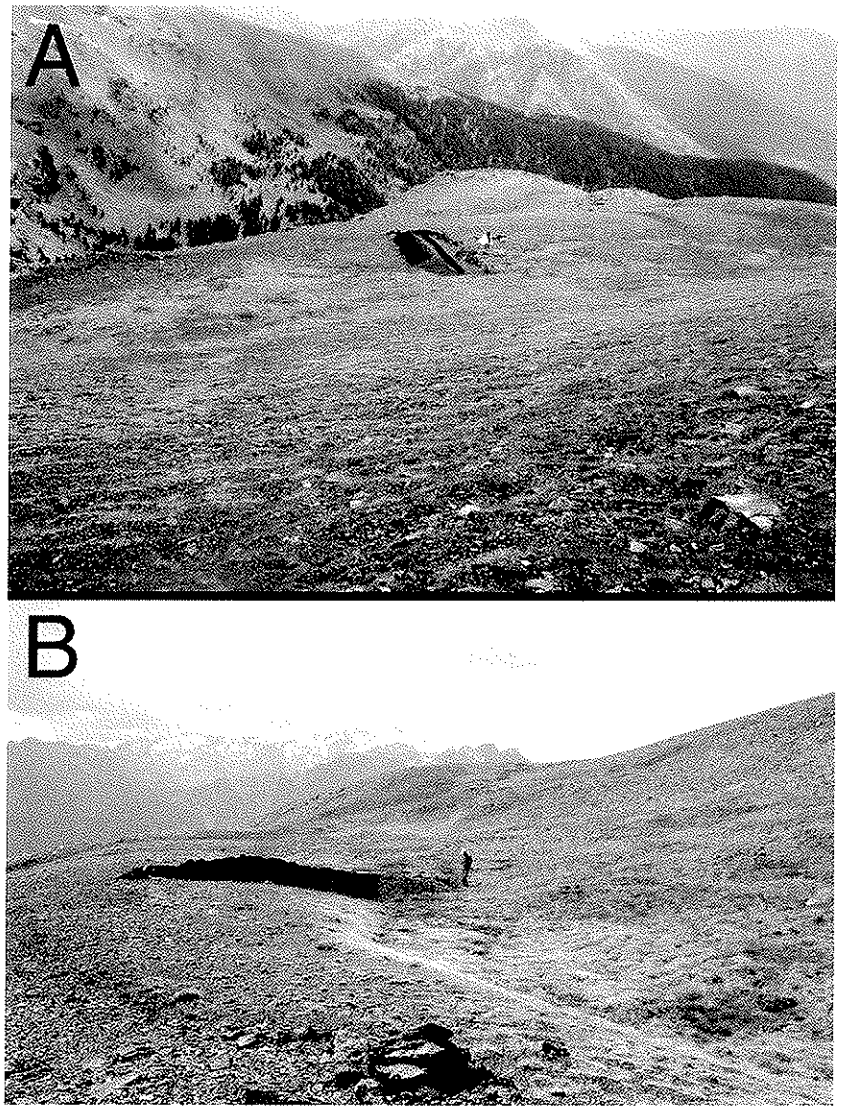

Fig. 7: (A): General view of the trench and sackung scarp and trough. The sharp linear change from turf-covered ground to bare bedrock coincides with the fault F1 of the trench. (B) Longitudinal view of the sackung scarp and trough. An en echelon sackung scarp in the background and located at a higher elevation.

The oldest depositional sequence of the trough fill (Ia and Ib) lies on bedrock or regolith in the hanging wall of fault F1 (Fig. 8). The lower unit of this sequence (Ia) consists of subangular and poorly sorted granule and pebble gravels with a sandy and clay matrix. This unit reaches a maximum thickness of 30 cm between stations 7-8 of the log horizontal scale. The upper unit is a dark brownish grey clay with greater thickness in the downthrown side of fault F2 (35-40 cm) than in the upthrown side, where it has been partially eroded. A charcoal sample collected in the hanging wall of fault F2 at about 20 cm above the base of the trough fill has yielded an age range of 15,190-14,900 cal. yr BP (error at 1σ). This stratigraphic sequence records the first depositional cycle in the sackung trough created by displacement on fault F1. Unit Ia is interpreted as a colluvial deposit shed from a scarp created by displacement on fault F1. The lacustrine unit Ib indicates that the sackung trough hosted an enclosed depression with a pond from its first stage of development. Units Ia and Ib are offset by faults F1 and F2, as well as by the three subsidiary normal faults mapped between F1 and F2. These structures, not obvious in the densely jointed bedrock, have been inferred based on the steeped geometry of the top of the gravel unit Ia and the apparent concordant drape folding of the overlying and more ductile argillaceous unit Ib.

The second stratigraphic sequence is faulted by F2 and restricted to the hanging wall of this fault (Fig. 8). Its lower colluvial unit (IIa) is made up of subangular pebble and granule gravel with a clayish sand matrix. This unit records the erosion of a free face created by a second displacement event over fault F1. The top of the upper lacustrine unit of this depositional sequence (part of IIb-IIIb1) is defined by the base of the overlying colluvial wedge (IIIa) between F2 and station 6. North of station 6 we have not been able to identify any stratigraphic change that would allow us to map the limit between the second and third depositional sequences. For this reason, unit IIb-IIIb1 includes the upper unit of the second depositional sequence and the lower part of the upper unit of the third depositional sequence. Stratigraphically below the colluvial wedge IIIa, unit IIb-IIIb1 contains a 5 cm thick bed of subrounded granules with brown clay matrix affected by a synform with a minimum amplitude of 50 cm and axis at station 5. The origin of this structure could be related to fault drag and tilting associated to fault F2 and deformation of the ductile clay sediments over a hypothetical south dipping fault located somewhere below the northern limb of the synform. Part of the amplitude of the synform could be syndepositional if the bed was accumulated on the concave bottom of a pond. An age range of 8,370-8,320 cal. yr BP (error at 1σ) has been obtained from charcoal fragments found near the base of unit IIb-IIIb1.

The youngest stratigraphic sequence truncates fault F2 and overlie unconformably unit Ib and unit IIb-IIIb1 south of station 6 (Fig. 8). As it has been indicated above, we have not been able to map the base of this stratigraphic sequence N of station 6 due to the massive nature of the argillaceous pond facies. Nonetheless, the angular unconformity identified in the "active margin" of the trough might grade into a conformable contact towards the depositional axis of the trough. The lower unit of this depositional sequence (IIIa) corresponds to a 80 cm thick colluvial wedge composed of subangular pebble granule gravel with a rough fabric inclined towards the sackung trough. This unit is juxtaposed to bedrock of the upthrown block of F1. The boundary between these two units, located over F1,

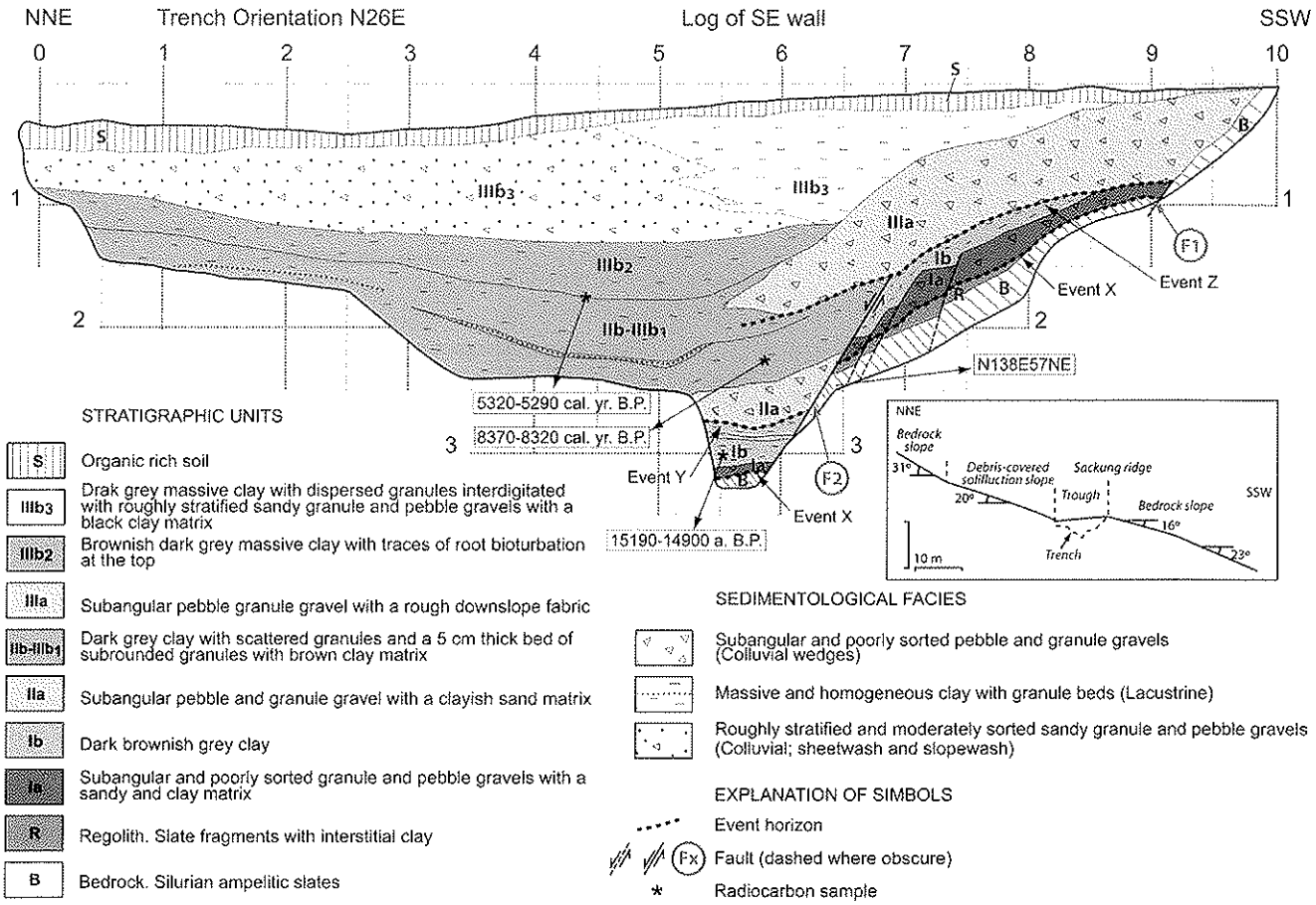

Fig. 8: Log of the SE wall of the trench and topographic profile of the slope at the trench site. Calendar ages correspond to ranges at 1σ. The location of the trench is shown in figures 3 and 6.

has been interpreted as a depositional free face contact based on the lack of shear fabrics and its relatively low inclination (~50°). The wedge-like geometry of the "tip" of the colluvial wedge IIIa between stations 5.5 and 6 is interpreted as a sharp lateral facies change that records a slight progradation of the colluvial wedge over the lacustrine facies and later expansion of the lacustrine deposits over the colluvial facies. Unit IIIa records the rejuvenation of the sackung scarp and trough by displacement on faults F1 and F2. The lacustrine upper term of the youngest depositional sequence corresponds to the upper part of unit IIb-IIIb1, and units IIIb2 and IIIb3. Units IIb-IIIb1 and IIIb2 are separated by an oxidation surface less than 0.5 cm thick that may represent a desiccation episode of the pond. Charcoal associated with this oxidation horizon that overlaps unit IIIa has yielded an age interval of 5,320-5,290 cal. yr BP (error at 1σ). Unit IIIb2, up to 50 cm thick, is composed of brownish dark grey massive clay with traces of root bioturbation at the top filled with sediment derived from the overlying unit. Unit IIIb3, about 1 m thick, consists of dark grey massive clay with scattered granules (lacustrine facies) interdigitated with roughly stratified sandy granule and pebble gravels with a black clay matrix derived from the northern margin of the trough (sheetwash and slopewash facies). Units IIIb2 and IIIb3 overlap unit IIIa reflecting the expansion of the pond over the colluvial wedge as detrital input decreased as a consequence of the degradation of the sackung scarp (Fig. 8). The sharp change in the depositional style occurred between units IIIb2 and IIIb3 without any evidence of deformation might be attributed to climate change or to natural or anthropogenic reduction in the vegetation cover of the slopes. The top of the trench walls shows an organic-rich soil up to 20 cm thick (unit S).

4.4. Trench interpretation

Three displacement events have been inferred based on the colluvial wedge stratigraphy and fault truncation relationships observed in the trench. The sequence of faulting events and depositional cycles has been depicted in a series of diagrams (Fig. 10). For simplification, these sketches do not incorporate the ductile deformation and tilting observed in the trench and assume a constant horizontal geometry for the bottom of the pond developed in the sackung trough.

The first displacement event (event X) corresponds to the faulting event that created the sackung scarp and trough (Fig. 10). Surface rupture on fault F1 created an antislope scarp high enough to generate a colluvial wedge (Ia) more than 30 cm thick and an enclosed basin with lacustrine deposition (IIb). The thickness of the first depositional sequence (40 cm)

provides a minimum value for the total vertical displacement and accommodation space created in this first event. The radiocarbon age obtained from unit Ib, 20 cm above the base of the trough, provides a minimum age of 15,190-14,900 cal. yr BP for event X (Fig. 8). A rough estimate of ca. 16.9 ka can be obtained for the age of the sackung trough by extrapolation to the bottom of the trough fill using the sedimentation rate calculated with the two youngest calendar ages. Regretfully, the lack of reliable chronological information on the glacial evolution of the El Ubago valley precludes establishing any relationship between this faulting event and the debutressing of the slopes induced by the retreat of the glacier.

The second and penultimate displacement event (PE, event Y) is recorded by the sharp change from lacustrine to colluvial deposition that represents the base of unit IIa (event horizon Y). Reactivation of fault F1, and possibly displacement on the minor failures mapped between F1 and F2, rejuvenated the sackung scarp causing the deposition of a colluvial wedge (IIa) more than 40 cm thick over the pond (Figs. 8 and 10). The calendar ages obtained from units Ib and IIb-IIIb1 provide a poorly constrained bracketing calendar age of 15-8.3 ka for event Y. The depositional sequence induced by this event, defined by the bases of units IIa and IIIa, reaches 90 cm in thickness. This figure provides a minimum measure for the total vertical displacement attained in this event, assuming that subsidence between displacement events was null or negligible. This assumption is supported by the fact that the unconformity that truncates fault F2, more than 5.3 ka old, does not show any evidence of deformation (Fig. 8).

Both faults F1 and F2, and possibly the subsidiary failure planes located between them, underwent displacement in the third and most recent deformation event (MRE, event Z). The collapse of the free face, partially underlain by unconsolidated deposits, produced a new colluvial wedge (IIIa) that truncates fault F2 (Figs. 8 and 10). Most likely, the tilting that displays the block between faults F1 and F2 occurred in this event as suggests the inclination towards the trough of the colluvial wedge IIIa. Fault F2, with a vertical displacement of about 100 cm, deformed the two previous depositional sequences and possibly contributed to the formation of the syncline that displays unit IIb-IIIb1 below unit IIIa. Part of the amplitude of this fold could be syndepositional as suggests the concave base of the units deposited after the MRE. Vertical offset on fault F1 was most likely higher than the thickness of colluvial wedge IIIa (80 cm). The thickness of the third depositional sequence provides a minimum vertical displacement of 175 cm for the MRE. The available calendar ages provide a poorly constrained time bracket of 8.3-5.3 ka for this event. This time interval overlaps with the ages obtained for the creation of the sackung features in Vallibierna (5.9 ka) and Estós (7.8-7.6 ka) sites and with the time range of 5.6-2.7 ka obtained for the displacement event recorded at the Vallibierna site [4], located 2.2 km to the NE.

The vertical separation of 3.2 m measured on the top of the bedrock and the age estimated for the sackung trough and scarp by extrapolation (16.9 ka) yield a minimum vertical displacement rate of 0.19 mm/yr. This figure may be significantly lower than the actual value due to the following reasons: (a) The trench does not exposes all the deformation. The top of the bedrock dips about 7° to the N for an unknown distance in the hanging wall of fault F2. (b) An originally horizontal geometry is implicitly assumed for the top of the bedrock before the creation of the sackung on an inclined bedrock slope. (c) The easily erodable slate bedrock has undergone significant erosion in the footwall of fault F1.

Fig. 9: Fault plane F2 exposed in the NW wall of the trench. The plane was coated with a striated film of clay.

The thickness of the depositional sequences (40, 90, 180 cm) and of the colluvial wedges (>30, >40, 80 cm) indicate an increasing amount of deformation with each displacement event. A similar trend has been inferred by McCalpin and Hart [9] in a ridge top depression in the San Gabriel Mountains of California (Blue Ridge site). As these authors interpret, such a trend may be related to the progressive weakening of the slopes by each successive gravitational failure event (strain softening). On the other hand, the age of the MRE (event Z) and the subdued morphology of the sackung reveals that this feature was not reactivated during the historical damaging seismic events recorded in the area, including the Ribagorza earthquake of 1373 (M_w 6.2), whose epicentral area was located at about 14 km from the study area [77, 61]. This indicates that the ground acceleration caused by those earthquakes at the site was below the equilibrium threshold of the sackung slope.

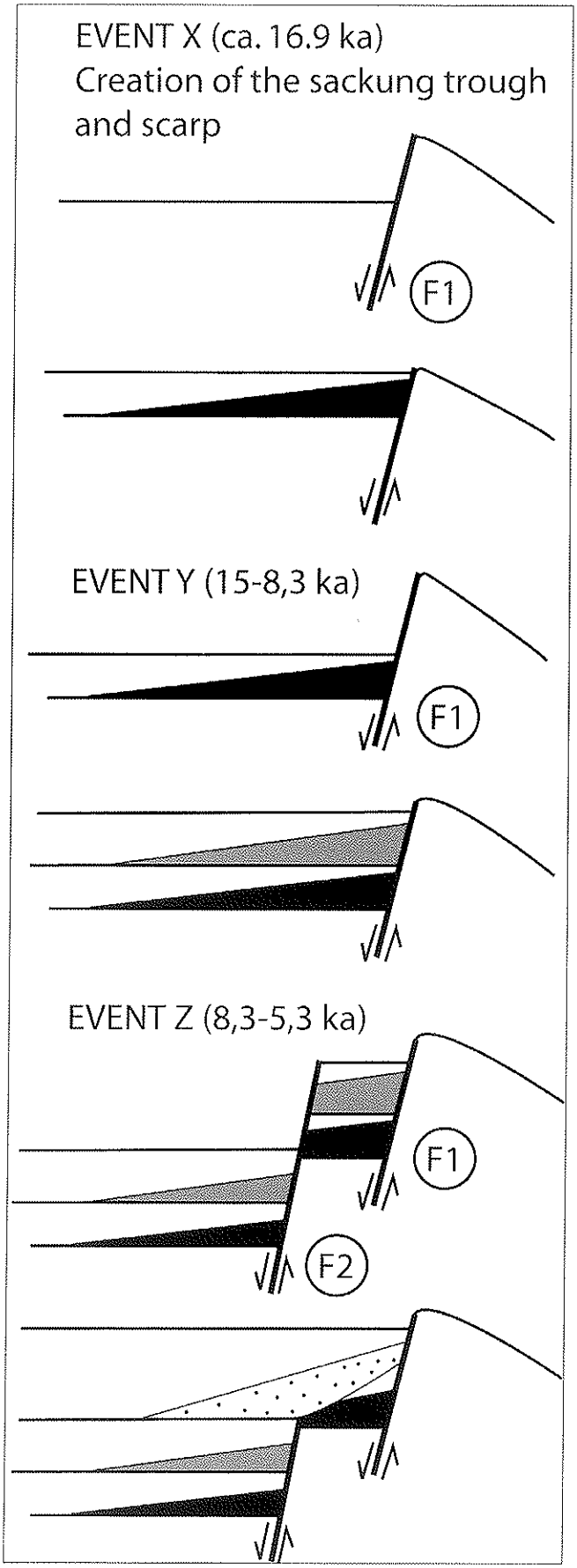

Fig. 10: Simplified diagrams showing the inferred sequence of faulting events and depositional episodes. These sketches do not incorporate ductile deformation, tilting and the subsidiary failure planes and assume a constant horizontal geometry for the bottom of the pond developed in the sackung trough.

5. Discussion

Four main external factors could be invoked to explain the episodic displacement recorded in the studied sackung: (a) Stress release due to glacial retreat; (b) Postglacial fluvial downcutting and undermining; (c) Climatically-induced water table rise; (d) Strong seismic shaking.

(a) Regretfully, there is no direct chronological information on the glacial evolution of the El Ubago valley. According to the glacial chronology proposed by Bordonau *et al.* [83], the studied sackung was created before the deglaciation of the valley. Following the chronological framework proposed by Pallás *et al.* [84] for the adjacent Noguera Ribagorzana valley, the temporal relationship between the deglaciation of the El Ubago valley (pre-12 ka) and the formation of the sackung scarp (ca. 16.9 ka) cannot be ruled out. Obviously, deglaciation-induced unloading can not be invoked to explain the penultimate and the most recent events identified in the sackung trench.

(b) Fluvial incision and undermining can be ruled out since the evidence of downcutting and lateral erosion in the El Ubago Stream is minimal compared with the size of the slope and the volume affected by deep-seated gravitational deformation.

(c) Despite deep-seated gravitational slope deformations are not as sensitive to climatic factors as small and shallow mass wasting processes, some authors hypothesize that the kinematics of sackung features may be controlled by hydroclimatic factors that lead to an increase in the pore water pressure (e.g. [86]). Johnson and Cotton [20] document the aseismic reactivation of a ridge top graben in the Santiago landslide (Aneheim Hills, California) during a period of high water table associated with intense rainfall. Additionally, some works document a reasonable temporal correlation between phases of higher landslide activity, including deep-seated mass movements, and specific climatic periods (e.g. [87, 88]). However, as Moya *et al.* [89] point out, the geochronological data on landslides in the Pyrenees is to scarce for the identification of temporal clusters. It would be also interesting to correlate the failure events inferred for the studied sackung with other paleoclimatic proxies (e.g. [90]). However, the ages obtained for those events are not tight enough to establish any significant temporal relationship. The age of the first failure event has been estimated by extrapolation and the bracketing ages of the penultimate and most recent displacement events cover long time spans (6.7 and 3 kyr). Consequently, the temporal and causal relationship between the displacement events recorded in the sackung and climatic triggers cannot be demonstrated or ruled out.

(d) Several arguments suggest that the creation and subsequent recurrent reactivation of the studied sackung have been triggered by strong seismic shaking:

(a) In this sector of the Pyrenees, the sackung features show a clear spatial association with the seismogenic North Maladeta Fault (Ortuño, pers. comm.), strongly suggesting that their origin and kinematics is controlled by large earthquakes generated on this structure. McCalpin and Hart [9] determined that the frequency of sackung occurrence, as it happens with other slope failures, increases with decreasing distance to active faults.

(b) The recurrence of displacement events of about 5.6 kyr, seems to be more consistent with the expectable millennial recurrence interval of large morphogenetic earthquakes in the area, than with the return period of climatic events.

(c) According to the glacial chronology proposed by Bordonau *et al.* [9], the generation of the sackung scarps previously studied in the neighbouring Estós and Vallibierna valleys occurred more than 5 kyr after the retreat of the glaciers [4].

Regretfully, we cannot demonstrate or invalidate the hypothesis of the coseismic displacement for our studied sackung due to the lack of independent paleoseismic information and the poor time constraints obtained for the displacement events [13, 9]. However, we consider that the presented data supports this postulate, which constitutes an interesting challenge for further investigations. Although evidence of coseismic displacement associated with sackung would not provide information on the seismic source and the earthquake magnitude [91], it might help to improve the catalogue of large paleoearthquakes providing information on earthquake recurrence intervals and the age of the MRE. For example, if the displacement events recorded in the analysed sackung would correspond to secondary paleoseismic evidence (as defined by McCalpin and Nelson, [92]), we could speculate that the recurrence of large earthquakes, most likely with an intensity at the site higher than that of the 1373 event, is on the order of 5.6 kyr. We could also indicate that the MRE with an intensity high enough to cause the gravitational failure of the slope would have an age range of 8.3-5.3 ka. This kind of inferences would be of great interest from the seismic hazard perspective [9], especially in an area like the Pyrenees, where the geomorphic and stratigraphic markers of neotectonic and paleoseismic activity are very scarce, largely due to intensive recent glaciation.

6. Conclusions

The northern slopes of the El Ubago glacial valley have been affected by post-glacial gravitational deformation and landslides. Deep-seated gravitational slope deformation is manifested at the surface by outward bulging, ridge top depressions, twin ridges, uphill- and down-hill facing scarps, a large graben depression and a collapse sinkhole. The length of the antislope scarps range from 60 to 720 m. The area affected by gravitational deformation covers approximately 4.4 km^2 and may involve a volume as large as 600 hm^3.

The trenched sackung trough and scarp have been created primarily by dip-slip displacement on failure planes dipping into the slope. The three depositional sequences of the trough fill, each consisting of a lower colluvial wedge unit and an upper lacustrine unit, record three displacement events followed by long periods of quiescence. The timing of the first faulting event (event X), responsible for the creation of the sackung, has been estimated by extrapolation at 16.9 ka. It has not been possible to establish any chronological relationship between this event and the deglaciation of the valley, of unknown age. The timing of the PE and the MRE faulting events (Events Y and Z) have been constrained at 15-8.3 and 8.3-5.3 ka. The scarcity of datable material in the trough fill has not allowed us to provide tighter bracketing ages. The age range of event Y overlaps with the ages obtained for the creation of the sackung features in Vallibierna (5.9 ka) and Estós (7.8-7.6 ka) sites and with the time range of 5.6-2.7 ka obtained for the displacement event recorded at the Vallibierna site [4], located at about 2 km on the other flank of the same ridge. In addition, the amount of deformation increases in each successive event. This trend could be related to the progressive weakening of the slopes caused by recurrent deformation events. The available data has allowed us to calculate a minimum vertical slip rate of 0.19 mm/yr for the sackung scarp and a recurrence interval of about 5.6 kyr for the faulting events.

Episodic displacement in the studied sackung with a millennial recurrence interval and the spatial association of the sackung features in this sector of the Pyrenees with the North Maladeta Fault, suggests that the generation and reactivation of the sackung scarps in the area could be controlled by strong seismic shaking. Such a potential secondary paleoseismic record could be of great utility for seismic hazard assessments in the Pyrenees, where intense glacial erosion and possibly the blind or buried character of seismogenic faults makes difficult to perform conventional paleoseismic investigations.

Acknowledgements

The authors would like to thank to Mr. Ramón Bardají (Servicio Provincial de Medio Ambiente, Huesca) and to the City Hall of Benasque village for granting permission to dig the trench in the vicinity of the Posets-Maladeta protected area. The investigation has been founded by the Italy-Spain Integrated Action "Landslide hazard assessment for a proper land-use planning in alpine areas under tourist pressure" (2006-07) funded by the Spanish and Italian governments. The manuscript has been improved thanks to the meticulous reviews carried out by Dr. James P. McCalpin, Alvaro González and three anonymous reviewers.

References

[1] Varnes, D.J., Radbruch-Hall, D.H., Savage, W.Z., Topographic and structural conditions in areas of gravitational spreading of ridges in the western United States, U.S. Geological Survey Professional Paper 1496, 1989, 28 p.

[2] McCalpin, J.P., Irvine, J.R., Sackungen at the Aspen Highlands ski area, Pitkin County, Colorado, Environmental and Engineering Geoscience 1 (1995) 277-290.

[3] McCalpin, J.P., Criteria for determing the seismic significance of sackungen and other scarplike landforms in mountanious regions, in: Techniques for identifying faults and determining their origins, U.S. Nuclear Regulatory Comission, Washington, 1999a, pp. 2.55-2.59.

[4] Gutiérrez-Santolalla, F., Acosta, E., Ríos, S., Guerrero, J., Lucha, P., Geomorphology and geochronology of sackung features (uphill-facing scarps) in the Central Spanish Pyrenees, Geomorphology 69 (2005) 298-314.

[5] Mahr, T., Deep-reaching gravitational deformations of high mountain slopes, Bulletin of the International Association of Engineering Geology 16 (1977) 121-127.

[6] Radbruch-Hall, D.H., Gravitational creep of rock masses on slopes, in: Voight, B. (Ed.), Rockslides and avalanches, 1, Natural Phenomena, Developments in Geotechnical Engineering, Elsevier, Amsterdam, vol. 14A, 1978, pp. 607-657.

[7] Agliardi, F., Crosta, G., Zanchi, A., Structural constraints on deep-seated slope deformation kinematics, Engineering Geology 59 (2001) 83-102.

[8] Bordonau, J., Vilaplana, J.M., Géomorphologie et tectonique récente dans le Val d'Aran (zone axiale des Pyrénées Centrales, Espagne), Revue de Géologie Dynamique et de Géographie Physique 27 (1986) 303-310.

[9] McCalpin, J.P., Hart, E.W., Ridge-top spreading features and relationship to earthquakes, San Gabriel Mountain region, southern California. Parts A and B, National Earthquake Hazard Reduction Program, U.S. Geological Survey, Technical report, 2002, 44 p.

[10] Bovis, M.J., Rock-slope deformation at Affliction Creek, southern Coast Mountains, British Columbia, Canadian Journal of Earth Sciences 27 (1990) 243-254.

[11] Ponti, D.J., Wells, R.E., Off-fault ground ruptures in the Santa Cruz Mountains, California: Ridge-top spreading versus tectonic extension during the 1989 Loma Prieta earthquake, Bulletin of the Seismological Society of America 81 (1991) 1480-1510.

[12] Onida, M., Tibaldi, A., Forcella, F., Galadini, F., Analysis of deep-seated slope deformations by paleoseismic technique, in: Girard, J.; Liebman, M.; Breeds, Ch., Doe, Th. (Eds.), Proceedings of the Fourth North American Rock Mechanics Symposium, Balkema, Rotterdam, 2000, pp. 515-521.

[13] Onida, M., Galadini, F., Forcella, F., Application of paleoseismological techniques to the study of Late Pleistocene-Holocene deep-seated gravitational movements at the Mortirolo Pass (central Alps, Italy), Netherlands Journal of Geosciences/Geologie en Mijnbouw 80 (2001) 209-227.

[14] Bovis, M.J., Uphill-facing (antislope) scarps in the Coast Mountains, southwest British Columbia, Geological Society of America Bulletin 93 (1982) 804-812.

[15] McCleary, J., Dohrenwend, J., Cluff, L., Hanson, K., 1872 earthquake studies, Washington public power supply system Nuclear Project Numbers 1 and 4, Woodward-Clyde Consultants, San Francisco, 1978, 75 p. unpublished report.

[16] Tabor, R.W., Origin of the ridge-top depressions by large-scale creep in the Olympic Mountains, Washington, Geological Society of America Bulletin 82 (1971) 1811-1822.

[17] Pasuto, A., Soldati, M., Rock spreading, in: Dikau, R., Brunsden, D., Schrott, L., Visen, M-L. (Eds.), Landslide recognition. Identification, movement and causes, Wiley, Chichester, 1996, pp. 122-136.

[18] Beck, A.C., Gravity faulting as a mechanism of topographic adjustment, New Zealand Journal of Geology and Geophysics 11 (1968) 191-199.

[19] Tibaldi, A., Rovida, A., Corazzato, C., A giant deep-seated slope deformation in the Italian Alps studied by paleoseismological and morphometric techniques, Geomorphology 58 (2004) 27-47.

[20] Johnson, Ph.L., Cotton, W.R., The Santiago Landslide and associated ridge-top graben (sackungen): Implications for paleoseismic studies, Environmental and Engineering Geoscience 11 (2005) 5-15.

[21] Cotton, C.A., Tectonic scarps and fault valleys, Geological Society of America Bulletin 61 (1950) 717-757.

[22] Dramis, F., Sorriso-Valvo, M., Deep-seated gravitational slope deformations, related landslides and tectonics, Engineering Geology 38 (1994) 231-243.

[23] Kellogg, K.S., Thrust-induced collapse of Mountains. An example from the "Big Bend" region of the San Andreas Fault, Western Transverse Ranges, California, U.S. Geological Survey Scientific Investigation Report 2004-5206, 2004, 16 p.

[24] Eusden, J., Pettinga, J.R., Campbell, J.K., Structural collapse of a transpressive hanging-wall fault wedge, Charwell region of the Hope Fault, South Island, New Zealand, New Zealand Journal of Geology & Geophysics 48 (2005) 295-309.

[25] Gutiérrez, F., Bruhn, R.L., McCalpin, J.P., Guerrero, J., Lucha, P., Evidence of compressional active tectonics in Ragged Mountain Fault (Southern Alaska). European Geosciences Union General Assembly, Geophysical Research Abstracts, Vol. 9, (2007) 01780.

[26] Dramis, F., Blumetti, A.M., Some considerations concerning seismic geomorphology and paleoseismology, Tectonophysics 408 (2005) 177-191.

[27] Varnes, D.J., Radbruch-Hall, D.H., Varnes, K.L., Measurement of ridge spreading movements (sackungen) at Bald Eagle Mountain, Lake County, Colorado, 1975-1989, U.S. Geological Survey, Open file report 90-543, 1990, 13 p.

[28] Varnes, D.J., Coe, J.A., Godt, J.W., Savage, W.Z., Savage, J.E., Measurement of ridge-spreading movements (sackungen) at Bald Eagle Mountain, Lake County, Colorado, II: cotinuation of the 1975-1989 measurements using a Global Positioning System in 1997 and 1999, U.S. Geological Survey, Open file report 00-205, 2000, on-line edition.

[29] Bovis, M.J., Evans, S.G., Rock slope movements along the Mount Currie "fault scarp", Southern Coast Mountains, British Columbia, Canadian Journal of Earth Science 32 (1995) 2015-2020.

[30] Evans, S.G., Clague, J.J., Origin and activity of antislope scarps in the mountains of southwestern British Columbia, Geological Society of America Abstracts with Programs 35, 6 (2003) 310.

[31] Beget, J.E., Tephrochronology of antislope scarps on an alpine ridge near Glacier Peak, Washington, U.S.A., Arctic and Alpine Research 17, 2 (1985) 143-152.

[32] Thompson, S.C., Clague, J.J., Evans, S.G., Holocene activity of the Mt. Currie scarp, Coast Mountains, British Columbia, and implications for its origin, Environmental and Engineering Geoscience 3 (1997) 329-348.

[33] Hewitt, K., Clague, J.J., Orwin, J.F., Legacies of catastrophic rock slope failures in mountain landscapes, Earth-Science Reviews 87 (2008) 1-38.

[34] Voight, B., Causes and consequences of eruptions of Andesite volcanoes, *Philosophical Transactions: Mathematical, Physical and Engineering Sciences,* 358 (2000) 1663-1703.

[35] Mège, D., Peulvast, J-P., Masson, Ph., A planetary example of tectonic inversion: folding and thrusting in the Valles Marineris Graben system of Mars, Lunar and Planetary Science, XXXVI, Abstract No. 1772, 2005.

[36] Ego, F., Sébrier, M., Carey-Gailhardis, E., Beate, B., Do the Billecocha faults (Ecuador) reveal extension due to lithospheric body forces in the Northern Andes, Tectonophysics 265 (1996) 255-273.

[37] Pan, E., Amadei, B., Stresses in an anisotropic rock mass with irregular topography, Journal of Engineering Mechanics 120 (1994) 97-119.

[38] Kinakin, D., Stead, D., Analysis of stress distributions in natural ridge forms: Implications for rock slope deformation mechanisms, Geomorphology 65 (2005) 85-100.

[39] Harp, E.L., Jibson, R.W., Landslides triggered by the 1994 Northridge California earthquake, Bulletin of the Seismological Society of America 86 (1996) S319-S332.

[40] Persaud, M., Pfiffner, O.A., Active deformation in the eastern Swiss Alps: post-glacial faults, seismicity and surface uplift, Tectonophysics 385 (2004) 59-84.

[41] Hippolyte, J-C., Brocard, G., Tardy, M., Nicoud, G., Bourlès, D., Braucher, R., Ménard, G., Souffaché, B., The recent fault scarps of the Western Alps (France): Tectonic surface ruptures or gravitational sackung scarps? A combined mapping, geomorphic, levelling, and ^{10}Be dating approach, Tectonophysics 418 (2006) 255-276.

[42] Paolucci, R., Amplification of earthquake ground motion by steep topographic irregularities. Earthquake Engineering and Structural Dynamics 31 (2002) 1831–1853.

[43] McCalpin, J.P., Episodic earthquake-induced movement on the Stillwater scarp "sackung", central Nevada, Geological Society of America Abstracts with Programs 31, 7 (1999b) 474.

[44] Wallace, R.E., Fault scarps formed during the earthquakes of October 2, 1915, Pleasant Valley, Nevada, and some tectonic implications, U.S. Geological Survey Prof, Paper 1274-A, 1984, 33 p.

[45] Nolan, J.M., Weber, G.E., Evaluation of surface cracking caused by the 1989 Loma Prieta earthquake, Santa Cruz County, California: Case histories, in: Sharma, S. (Ed.), Proceddings of the 28th Symposium on Engineering Geology and Geotechnical Engineering, University of Idaho, 1992, pp. 272-286.

[46] Nolan, J.M., Weber, G.E., Evaluation of coseismic ground cracking accompanying the earthquake: Trenching studies and case histories. The Loma Prieta, California, earthquake of October 17, 1989; landslides, U.S. Geological Survey Professional paper 1551-C, 1998, pp. 145-163.

[47] Tarr, R.S, Martin, L., Earthquakes at Yakutat Bay, Alaska, in September, 1899, U.S. Geological Survey Professional Paper, 69, 1912, 136 p.

[48] Tocher, D., Movement on the Fairweather fault and field investigation of southern epicentral region, Seismological Society America Bulletin 50 (1960) 267-292.

[49] Plafker, G., Surface faults on Montague Island associated with the 1964 Alaska earthquake. U. S. Geological Survey Professional Paper 543-G (1967) 42.

[50] Jibson, R.W., Harp, E.L., Sculz, W., Keefer, D.K., Landslides triggered by the 2002 Denali Fault, Alaska, earthquake and the inferred nature of the strong shaking, Earthquake Spectra 20 (2004) 669-691.

[51] Blumetti, A.M., Neotectonic investigations and evidence of paleoseismicity in the epicentral area of the January-February 1703, Central Italy, earthquakes, Association of Engineering Geology Special Publication 6 (1995) 83-100.

[52] Dramis, F., Sorriso-Valvo, M., Two cases of earthquake-triggered gravitational spreading in Algeria and in Italy, Rend. Soc. Geol. It. 6 (1983) 7-10.

[53] Moro, M., Saroli, M., Salvi, S., Stramondo, S., Doumaz, F., The relationship between seismic deformation and deep-seated gravitational movements during the 1997 Umbria-Marche (Central Italy) earthquakes, Geomorphology 89 (2007) 297-307.

[54] Lyell, C.L., Principals of Geology, D. Appleton New York, 1874, 652 p.

[55] Gil Peña, I., Estructura alpina de la zona axial, in: Vera, J.A. (Ed.), Geología de España, IGME, Madrid, 2004, pp. 323-325.

[56] García-Sansegundo, J., Estratigrafía y estructura de la Zona Axial pirenaica en la transversal del Valle de Arán y de la Alta Ribagorza (Parte I), Boletín Geológico y Minero 102 (1991) 781-829.

[57] García-Sansegundo, J., Estratigrafía y estructura de la Zona Axial pirenaica en la transversal del Valle de Arán y de la Alta Ribagorza (Parte II), Boletín Geológico y Minero 103 (1992) 42-93.

[58] Barnolas, A., Pujalte, V., La Cordillera Pirenaica. Definición, límites y division, in: Vera, J.A. (Ed.), Geología de España, IGME, Madrid, 2004, pp. 233-241.

[59] Nocquet, J.M., Calais, E., Geodetic measurements of crustal deformation in the western Mediterranean and Europe, Pure Appl. Geophys, 161 (2004) 661-681.

[60] Nicolas, M., Santoire, J.P., Delpech, P.Y., Intraplate seismicity: new seismotectonic data in Western Europe, Tectonophysics 179 (1990) 27-53.

[61] Susagna, T., Roca, A., Goula, X., Batlló, J., Analysis of macroseismic and instrumental data for the study of the 19 November 1923 earthquake in the Aran Valley (Central Pyrenees), Natural Hazards 10 (1994) 7-17.

[62] Olivera, C., Redondo, E., Lambert, J., Riera Melis, A., Roca, A., Els terratrèmols dels segles XIV i XV a Catalunya, Institut Cartogràfic de Catalunya, Monografies 30, 2006, 407 p.

[63] Dubos-Sallée, N., Nivière, B., Lacan, P., Hervouët, Y., A structural model for the seismicity of the Arudy (1980) epicentral area (Western Pyrenees, France), Geophysical Journal International 171, 1 (2007) 259–270.

[64] Giménez, J., Suriñach, E., Fleta, J., Goula, X., Recent vertical movements from high precision leveling data in Northeastern Spain. Tectonophysics, 263 (1996) 59-75.

[65] Stich, D., Serpelloni, E., Mancilla, F. L., Morales, J., Kinematics of the Iberia –Maghreb plate contact from seismic moment tensors and GPS observations, Tectonophysics, 426 (2006) 295-317.

[66] De Vicente, G., Cloetingh, S., Muñoz-Martín, A., Olaiz, A., Stich, D., Vegas, R., Galindo-Zaldivar, J., Fernández-Lozano, J., Inversion of moment tensor focal mechanisms for active stresses around Microcontinent Iberia: Tectonic implications, Tectonics, 27 (2008) TC1009.

[67] Alasset, P.-J., Meghraoui, M., Active faulting in the western Pyrénées (France): Paleoseismic evidence for late Holocene ruptures, Tectonophysics 409 (2005) 39-54.

[68] Carbon, D., Combes, P., Cushing, M., Granier, T., Grellet, B., Rupture de surface post-Pléistocène moyen dans le Bassin aquitain, CR Acad. Sci. Paris, série IIa, 320 (1995) 311-317.

[69] Klarica, S., Hervouët, Y., Bauer, J., Karst et extensions gravitaires d'altitude : le massif du Jaout (Pyrénées occidentales, France), Geologica Belgica, 4, 3-4 (2001) 213-229.

[70] Briais, A., Armijo, R., Winter, T., Tapponnier, P., Herbeck, A., Morphological evidence for Quaternary normal faulting and seismic hazard in the Eastern Pyrenees, Annales Tectonicae, IV, 1 (1990) 19-42.

[71] Philip, H., Bousquet, J.C., Escuer, J., Fleta, J., Goula, X., Grellet, B., Présence de failles inverses d'âge quaternaire dans l'Est des Pyrénées: implications sismotectoniques, C. R. Acad. Sci. Paris, 314, Tectonique, série II (1992) 1239-1245.

[72] Calvet, M., Régimes des contraintes et volumes de relief dans l'est des Pyrénées, Géomorphologie : relief, processus, environnement, 5, 3 (1999) 253-278.

[73] Goula, X., Olivera, C., Fleta, J., Grellet, B., Lindo, R., Rivera, L.A., Cisternas, A., Carbon, D., Present and Recent stress regime in the eastern part of the Pyrenees, Tectonophysics, 308, 4 (1999) 487-502.

[74] Rodríguez-Pascua, M.A., Estudios paleosismológicos en España: una revisión, Boletín Geológico y Minero 116 (2005) 203-216.

[75] Ortuño, M., Perea, H., Masana, E., Santanach, P, La falla Norte de la Maladeta, ¿fuente sísmica del terremoto de Vielha (11 de Noviembre de 1923)? Geotemas 6, 3 (2004) 171-174.

[76] Ortuño, M., Queralt, P., Martí, A., Ledo, J., Masana, E., Perea, H., and Santanach, P., The North Maladeta fault (Central Pyrenees) as the Vielha 1923 earthquake seismic source: recent activity revealed by geomorphological and geophysical research, Tectonophysics 453, 1-4 (2008) 246-262.

[77] Olivera, C., Riera, A., Lambert, J., Banda, E., Alexandre, P., Els terratrèmols de l'any 1373 al Pirineu. Effectes a Espanya i França, Servei Geològic de Catalunya, 1994, 220 p.

[78] Wells, D.L., Coppersmith, K.J., New empirical relationships among magnitude, rupture length, rupture area and surface displacement, Bulletin of the Seismological Society of America 84 (1994) 974-1002.

[79] Ortuño, M. and Santanach, P., Recent tectonic activity in high mountain regions: Scarps in the Maladeta Massif (Central Pyrenees), VI International Conference on Geomorphology, Zaragoza (Spain), 2005, pp. 295.

[80] Larrasoaña, J.C., Ortuño, M., Parés, J.M., Valero-Garcés, B., Bordonau, J., Copons, R., Mineral magnetic record of late Holocene environmental changes and seismic events in a high altitude glacio-lacustrine sequence (Lake Barrancs, Pyrenees), 4th International Limnogeology Congress, Barcelona, 2007, pp. 199-200.

[81] Ríos, L.M., Galera, J.M., Barettino, D., Mapa Geológico de España, Hoja de Benasque (180), Instituto Geológico y Minero de España, Madrid, 1997, 78 p.

[82] Bordonau, J., The Upper Pleistocene ice-lateral till complex of Cerler (Ésera valley, Central Southern Pyrenees; Spain), Quaternary International 18 (1993) 5-14.

[83] Bordonau, J., Serrat, D., Vilaplana, J.M., Las fases glaciares cuaternarias en los Pirineos, in: Cearreta, A., Ugarte, F.M. (Eds.), The Late Quaternary in the western Pyrenean region, Universidad del País Vasco, Bilbao, 1992, pp. 303-312.

[84] Pallàs, R., Rodés, A., Braucher, R., Carcaillet, J., Ortuño, M., Bordonau, J., Bourlès, D., Vilaplana, J.M., Masana, E., Santanach, P., Late Pleistocene and Holocene glaciation in the Pyrenees: a critical review and new evidence from ^{10}Be exposure ages, south-central Pyrenees, Quaternary Science Reviews 25 (2006) 2937-2963.

[85] Soldati, M., Deep-seated gravitational slope deformation, in: Goudie, A.S. (Ed.), Encyclopedia of Geomorphology, Routledge, London, 2004, pp. 226-228.

[86] Ambrosi, C., Crosta, G.B., Large sacking along major tectonic features in the Central Italian Alps, Engineering Geology 83 (2006) 183-200.

[87] Borgatti, L., Soldati, M., The influence of Holocene climatic changes on landslide occurrence in Europe, in: Rybár, J., Stemberk, J., Wagner, P. (Eds.), Landslides, A.A. Balkema Publishers, Lisse, 2002, pp. 111-116.

[88] González Díez, A., Salas, L., Díaz de Terán, J.R., Cendrero, A., Late Quaternary climate changes and mass movement frequency and magnitude in the Cantabrian region, Spain, Geomorphology 15 (1996) 291-309.

[89] Moya, J., Vilaplana, J.M., Corominas, J., Late Quaternary and historical landslides in the south-eastern Pyrenees, in: Matthews, J.A., Brunsden, D., Frenzel, B., Gläser, B., Weiß, M.M. (Eds.), Rapid mass movements as a source of climatic evidence for the Holocene, Paläoklimaforschung-Paleoclimate Research, 19 (1992) 55-73.

[90] González Sampériz, P., Valero Garcés, B.L., Moreno, A., Jalut, G., García-Ruiz, J.M., Martí Bono, C., Delgado Huertas, A., Navas, A., Otto, T., Dedoubat, J.J., Climatic variability in the Spanish Pyrenees during the last 30,000 yr revealed by the El Portalet sequence, Quaternary Research 66 (2006) 38-52.

[91] Jibson, R.W., Using landslides for paleoseismic analysis, in: McCalpin, J. (Ed.), Paleoseismology, Academic Press, London, 1996, pp. 397-438.

[92] McCalpin, J.P, Nelson, A.R., Introduction to Paleoseismology, in: McCalpin, J.P. (Ed.), Paleoseismology, Academic Press, New York, 1996, pp. 1-32